Journal of Applied Physics

More accurate parameterization of positron implantation depth profiles for the sensitivity range of positron-based characterization techniques

Cite as: J. Appl. Phys. **128**, 045105 (2020); https://doi.org/10.1063/5.0011021
Submitted: 17 April 2020 • Accepted: 19 June 2020 • Published Online: 23 July 2020

J. V. Logan, M. P. Short, P. T. Webster, et al.

Journal of Applied Physics ARTICLE scitation.org/journal/jap

More accurate parameterization of positron implantation depth profiles for the sensitivity range of positron-based characterization techniques

Cite as: J. Appl. Phys. **128**, 045105 (2020); doi: 10.1063/5.0011021
Submitted: 17 April 2020 · Accepted: 19 June 2020 ·
Published Online: 23 July 2020

J. V. Logan,[1,2,a)] M. P. Short,[1] P. T. Webster,[2] and C. P. Morath[2]

AFFILIATIONS

[1]Department of Nuclear Science and Engineering, Massachusetts Institute of Technology, 77 Massachusetts Ave., Cambridge, Massachusetts 02139, USA
[2]Air Force Research Laboratory, Space Vehicles Directorate, Kirtland AFB, New Mexico 87117, USA

[a)]**Author to whom correspondence should be addressed:** jvl2xv@mit.edu

ABSTRACT

Techniques that employ positron annihilation spectroscopy are powerful tools to investigate defect structures and concentrations in materials. A hindrance to experimental design and the interpretation of results lies in the lack of agreement in the literature concerning the proper form of the positron implantation profile, a function that determines the sensitivity range for all non-slow positron annihilation spectroscopy techniques. Employing the dominant ^{22}Na isotopic source, a positron implantation profile database of 270 common materials is published. The parameters for a novel implantation profile functional form providing superior agreement with simulation are derived. Finally, and most critically, an algorithm is presented and validated, which permits utilization of the published elemental implantation profile parameters to produce the positron implantation profile for any material of interest. This tool provides rapid calculation of the sensitivity range for all positron annihilation techniques, enabling more informed experimental design and more accurate knowledge of the spatial distribution of defects in materials.

https://doi.org/10.1063/5.0011021

I. INTRODUCTION

Positron annihilation spectroscopy (PAS) techniques yield insight into the concentration and structure of open volume defects in materials. Most implementations use unmoderated ^{22}Na positron sources.[1,2] The distribution of the PAS sensitivity as a function of depth depends on the depth distribution of positron annihilation in the material under characterization, which remains a point of contention in the literature.[1,3–10]

There is a lack of consensus in the field concerning the proper form of the positron annihilation probability as a function of distance normal to the sample surface, a distribution known as the positron implantation profile (PIP). This disagreement forces experimentalists to compare multiple published models in order to ensure consistency for their particular system of interest.[8,11] Furthermore, no systematic algorithm has been proposed to produce PIPs for an arbitrarily defined compound, even for simple binary semiconductors. This lack of an accepted implantation profile model leads to uncertainty in the following critical parameters for a wide range of materials under investigation: (1) material-dependent, effective sensitivity range of PAS, (2) required thickness of material to restrict positron annihilation within, and (3) technique sensitivity in comparison with the range of damage-causing radiation (e.g., in ion implantation studies).

This work allows experimentalists to answer these questions. First, a 270 material database of PIPs is published for a range of common materials. Second, the parameters for a novel, functional form providing superior agreement with simulation are published. Third, and most critically, an algorithm is presented and validated, which permits utilization of the published elemental implantation profile parameters to produce the PIP for any arbitrarily defined material of interest.

II. BACKGROUND

Positron motion in condensed matter can be roughly partitioned into two stages: implantation/thermalization and diffusion. The final stage makes a negligible contribution to the spatial distribution of positron annihilation (contributing $<1\,\mu$m) despite the fact that it dominates the lifetime of the positron.[3] Upon traversing through and interacting with the material nuclei and electrons, positrons obtain a time-independent momentum distribution, representing thermal equilibrium with the host material. The depth distribution of thermalized positrons perpendicular to the source surface prior to the beginning of the diffusion stage defines the PIP, and this profile determines the sensitivity range for positron-based material characterization techniques. The subsequent diffusion depth distribution can be determined using the steady-state diffusion annihilation equation with the PIP as a source term. While thermal, positrons move in a random-walk manner, covering a volume occupied by approximately 10^9 atoms.[4,7,12,13]

In contrast to fast ions moving through materials, fast positrons, with energies in the keV–MeV range, follow a tortuous path and lose energy at a lesser rate. The dominant electrostatic Coulomb scattering interaction with orbital electrons has the potential to dramatically change the positron direction due to the equality of masses of the interacting particles. Because ions do not experience this degree of direction change upon scattering from material electrons, it is straightforward to define ion implantation range and straggle. For positrons, this is not the case. As the probabilistic scattering angle and energy loss associated with each scattering event are themselves complex functions of energy, the positron implantation profile does not have an analytical form. Heuristically, the absorption profile of positrons emitted with the energy spectrum typical of β^+ decay has been found to approximate an exponential because the lower energy positrons are absorbed in a smaller distance and higher energy positrons can propagate further.[14]

In 1951, Gleason *et al.*[15] measured the PIP as a function of depth (z) and described it using a single-exponential distribution with the decay coefficient dependent only upon the material density (ρ in g/cm^3) and maximum energy of the positrons in the radioisotope decay spectrum $E_{\max}$ (MeV),

$$\alpha^+ = 17\frac{\rho}{E_{\max}^{1.48}} \quad (\mathrm{cm}^{-1}). \tag{1}$$

Brandt and Paulin[16] later presented a similar parametrization,

$$\alpha^+ = (19.3 \pm 1.2)\frac{\rho}{E_{\max}^{1.28\pm0.11}} \quad (\mathrm{cm}^{-1}). \tag{2}$$

Mourino *et al.*[9] developed a single-exponential decay coefficient, which varied with both the material density as well as the material atomic number (Z) and the mean energy ($\overline{E}$ in MeV) of the positron profile,

$$\alpha^+ = 2.8\,Z^{0.15}\frac{\rho}{\overline{E}^{1.19}} \quad (\mathrm{cm}^{-1}). \tag{3}$$

This single-exponential PIP model remains the dominant functional form due to its universality despite repeated experimental demonstrations of its inability to capture the true PIP, which as shown in Fig. 5, is only single exponential over a limited range in depth.[3,5,9] Later, Płotkowski *et al.*[17] developed a two-term exponential form with the second term accounting for the true isotopic nature of positron emission in which $Ei()$ is the exponential integral function,

$$PIP(z) = e^{-z\alpha^+} + z\alpha^+ Ei(-z\alpha^+). \tag{4}$$

Saoucha presented a similar form but with differing short-range and long-range attenuation coefficients.[18] Numerous two-exponential fits have been proposed, but all suffer from similar limited ranges of applicability, only shown to work well for subsets of materials.[3,5] Dryzek and Singleton[3] developed a form that convolves a depth and energy dependent Gaussian $g(E, z)$ (or a modified Gaussian in later work by Dryzek and Sieracki[19]) with each energy in the β decay spectrum, as weighted by the likelihood of that decay energy $P(E)$,

$$PIP(z) = \int_0^{E_{\max}} P(E)g(E, z)dE. \tag{5}$$

Siemek and Dryzek[20] later developed a piece-wise parameterization, whereby the PIP takes on a single-exponential character beyond a critical thickness $d_0 \simeq 0.5/\alpha^+$, in which N is a normalization constant to ensure continuity,

$$PIP(z) = \begin{cases} \frac{N}{2}\left[e^{-2\alpha^+ z} + e^{-2\alpha^+ d_0}\right], & z \le d_0, \\ N\left[e^{-\alpha^+(z+d_0)}\right], & z > d_0. \end{cases} \tag{6}$$

The authors acknowledge the existence of a long-range region in the PIP, the functional form of which is not accounted for by this parameterization. Recent work proposes the existence of three regions within the PIP: a fast decay region, an exponential decay region to which the linear absorption coefficient is fit, and another fast decay region.[3] A single distribution, applicable to all materials, would be of superior practical utility, and previous failures in the literature to derive one warrant the inclusion of additional terms.

The majority of PIP modeling efforts assume encapsulation of the ^{22}Na source within thin Kapton foils (usually $8\,\mu$m in thickness). Due to the fact that there will be varying encapsulation methods, this limits the utility of these PIPs to the specific geometry modeled. Furthermore, this geometrical source arrangement is highly non-ideal in positron annihilation lifetime spectroscopy (PALS) experiments due to the fact that source lifetime components, including those from the Kapton encapsulation, must be very accurately estimated and subtracted from the positron lifetime spectrum. Its impact is arguably greater in Doppler broadening experiments because there is no method to take into account the source contribution to the broadened spectrum.[11] This source component contributes the dominant uncertainty to lifetimes obtained in PALS[21] and can be avoided through direct deposition of ^{22}Na on the sample of interest. For these reasons, this work provides a parameterization of the PIP in materials without any form of encapsulating foil.

III. METHODS

The GEANT4 Monte Carlo toolkit is employed to simulate PIPs in all materials.[22,23] For each simulation, a range cutoff of 1 nm is employed (a value that is internally converted into a production energy cutoff for each material under consideration). As PIPs are generally on the order of 100 s of μm, the impact of this cutoff is negligible. The PENELOPE (PENetration and Energy LOss of Positrons and Electrons) physics list, a customized physics list for low-energy interactions of light charged particles, is used to describe the physics of positron interactions. The precision of the electromagnetic processes incorporated into this toolkit has been extensively validated.[24] In this effort, the results are also validated with an additional intrinsic physics list, the Shielding physics list, and the results are found to agree to within statistical variation as shown in the Appendix. The recommended energy range for the PENELOPE physics list is 100 eV–1 GeV, but GEANT4 tracks positrons until a process (like annihilation) results in their death.[25] Given the stopping power of 100 eV positrons, they travel a minimal distance between 100 eV and thermalization.[26] 1 000 000 positrons are simulated for each material. The geometry of these simulations consists of a ^{22}NaCl salt cylinder 1 mm in radius and 1.25 nm in height, encased by two identical pieces of the material under test of thickness necessary to ensure that all positrons annihilate within the volume. The salt component radius is standard in experiments, and the height is determined by the requirement of a 10 μCi decay rate, assuming a virgin source and taking into account the specific activity of ^{22}Na. This arrangement is illustrated in Fig. 1. The use of GEANT4 for the determination of positron implantation profiles has been validated extensively in the literature through comparison with experimental results.[3–6,27–30]

As the radioisotope ^{22}Na is most commonly used in PAS techniques due to its uniquely well-suited decay characteristics of lifetime and coincident decay gamma emission, the β^+ spectrum for this decay is used for all simulations.[4,31] This spectrum has no precise analytical form; therefore, the parameterized spectrum is taken from ICRP Publication 107 (nuclear decay data for dosimetric calculations) and is plotted in Fig. 2. Both β^+ decays that the ^{22}Na nucleus can undergo are included in the analysis: 89.8% per decay 0.5456 MeV endpoint energy and 0.055% per decay 1.820 MeV endpoint energy.[32]

A selection of 270 common materials (detailed in the supplementary material) is simulated in order to produce an extensive library for general use and also to serve as a large dataset for effective fit parameterization. Following Monte Carlo simulations of the PIP, 1 μm bin width histograms are normalized to unity at the sample's surface and fit using a nonlinear least squares method using the trust-region optimization algorithm.[33] A summation of two, three, four, and five single exponentials is considered as a function of both distance into the material [μm] and distance into the material divided by the material density [μm/(g/cm^3)]. The four exponential expression is given in Eq. (7), which shows that each single-exponential term contributes two fit parameters: a vertical-axis intercept coefficient (A, C, E, G) and a characteristic slope in the exponent (B, D, F, H). For each fit expression, the

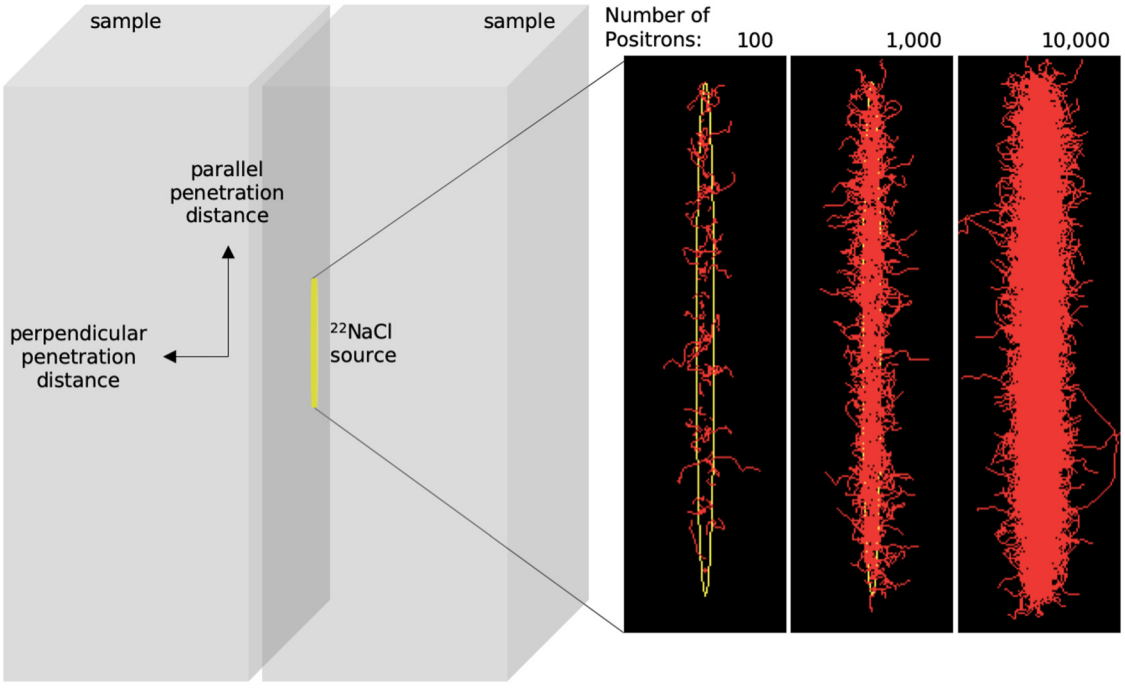

FIG. 1. GEANT4 geometry as simulated to obtain PIPs. (Left) Two identical materials (gray) surround the ^{22}NaCl salt cylinder (yellow), from which positrons are emitted. (Right) Positron tracks (red) simulated in the material for 100, 1000, and 10 000 incident positrons.

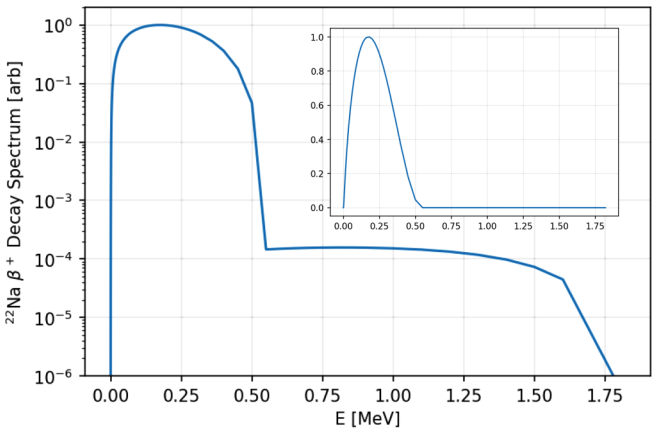

FIG. 2. Energy spectrum of β^+ particles emitted in the decay of the ^{22}Na nucleus. As this radioisotope is used for the majority of positron-based material characterization techniques, this spectrum is employed as an input for all PIP simulations.[4] ^{22}Na decays through two β^+ modes with the mean number of decays via each mode per nuclear transformation being 89.8% and 0.055%, respectively. The mean energies of emitted positrons for these modes are 0.2155 and 0.8350 MeV, respectively. The maximum (end point) energies of these positrons are 0.5456 and 1.820 MeV, respectively. The spectrum is taken from ICRP Publication 107 (nuclear decay data for dosimetric calculations), with more detail available in the supplementary material.[32]

simulated PIPs are fit in order of density with the optimum parameters from the previous material used as the initial condition for the next. As the fit quality is seen to improve with density, the fit is conducted in order of decreasing density. The resulting fits are approximately equivalent, showing that the improvement with the density is intrinsic to the material and not an artifact of the fitting algorithm. Additionally, two different weighting methods are considered: a weighting of the data by its value and a weighting of the data by the inverse of its value. The former increases the importance of low-depth, high-count points in the PIP, whereas the latter equalizes the importance of data that varies over orders of magnitude. The goodness-of-fit statistics for these two weighting options are presented in the supplementary material, which shows that the results are equivalent after a sufficient number of single exponentials are introduced to adequately characterize the complex PIP curve shape,

$$PIP(x) = Ae^{-Bx} + Ce^{-Dx} + Ee^{-Fx} + Ge^{-Hx}. \quad (7)$$

Physical knowledge of the PIP permits bounds to be set on the fitted coefficient variables. All exponentials are decaying; therefore, the characteristic slope parameters are bounded from 0 to ∞. Data normalization permits reduction of the number of vertical-axis intercept coefficients by one due to the implementation of a surface boundary condition.[33] As such, only three of the four vertical-axis intercept coefficients are fit in the model, with the final constrained to be equal to $G = 1 - (A + C + E)$. Furthermore, all counts must be positive and cannot exceed unity at the sample surface; therefore, all vertical-axis intercept coefficients are bound between 0 and 1. To maximize the likelihood of locating an optimal fit for each PIP, the best-fit minimization algorithm is conducted in 300 trials for each material, with the best fit in terms of the root mean square error (RMSE) being selected. The fit quality is seen to saturate at approximately 200 trials; therefore, the use of 300 trials helps maximize the likelihood of obtaining a true global minimum of the objective

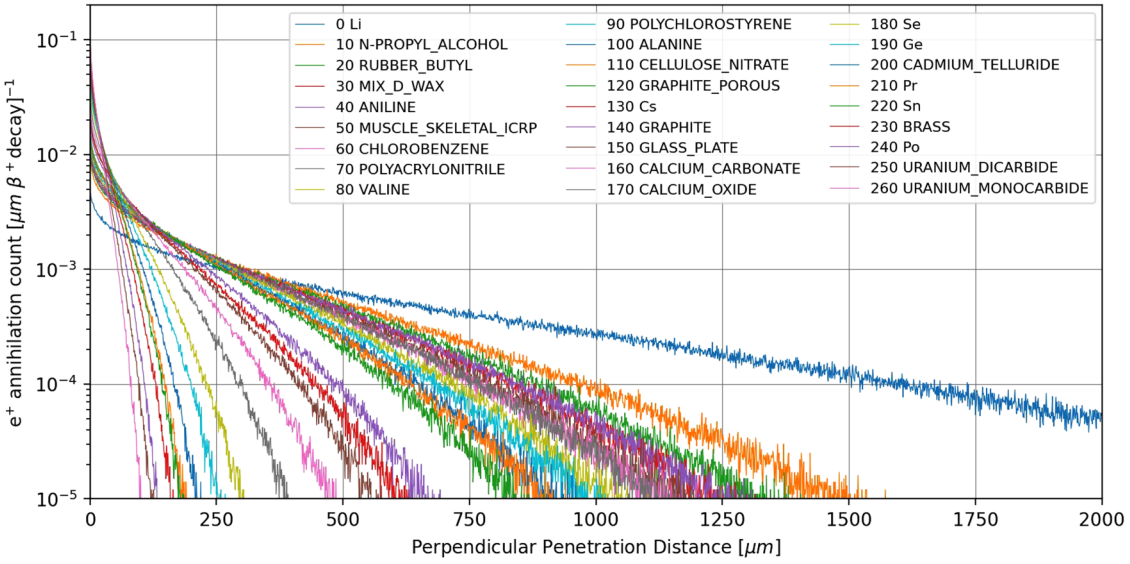

FIG. 3. PIPs for a subset of the 270 materials in the database of common materials (the density-ordered number given in the legend). The annihilation count is shown per incident positron per μm penetration perpendicular to the material surface. The entire dataset is from GEANT4 simulations and is used for subsequent validation of the PIP reconstruction algorithm as discussed in Sec. III. The tabular form of this data is found in the supplementary material.

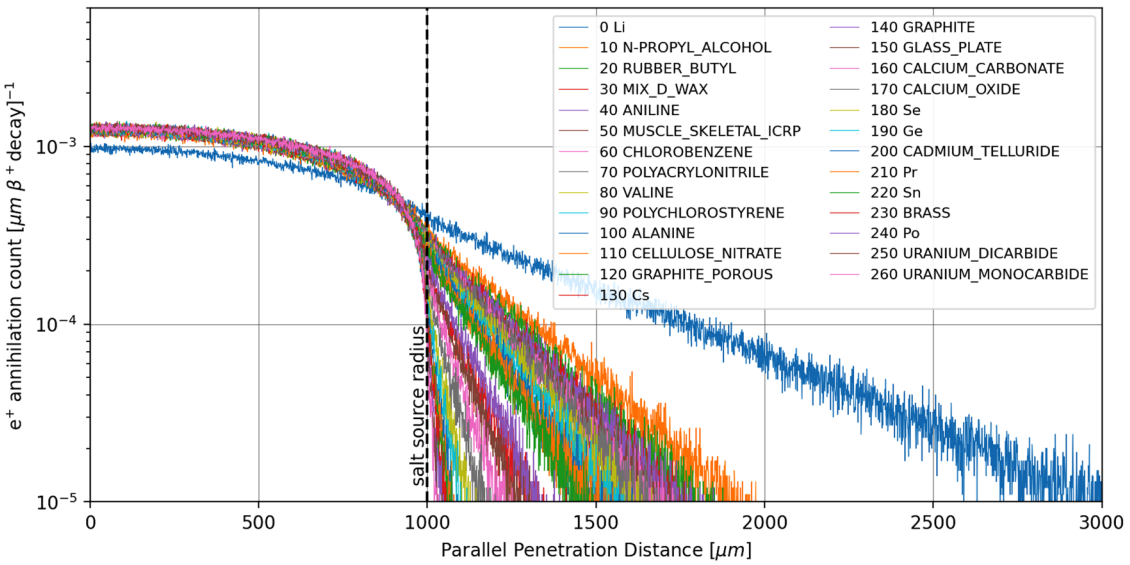

FIG. 4. PIPs for a subset of the 270 materials in the GEANT4 database of common materials (the density-ordered number given in the legend). The annihilation count is shown per incident positron per μm penetration parallel to the material surface. These results are from GEANT4 simulations as discussed in Sec. III. The tabular form of this data is found in the supplementary material.

function—the best fit. The quality of the fit is quantified in terms of the sum of squares error (SSE), RMSE, R^2, and adjusted R^2 parameters for all materials considered and functional fits. The fit residuals are also analyzed to ensure that the fit does not omit any major features in the data. This step proved to be particularly important, as it enabled determination of the best model to parameterize a PIP function for all materials. Following determination of the optimum functional form to the PIP, the coefficients are obtained for all materials, including all pure elements. Given these elemental parameters as input, a reconstruction algorithm is developed to transform these into PIPs for any arbitrary material of known composition. This reconstruction algorithm is validated using the aforementioned material database. To supplement the validation of this PIP reconstruction algorithm for materials of prime interest to the PAS analysis, the PIP is also simulated for a set of six binary semiconductor materials: GaN, ZnO, MgO, GaP, InAs, and InP. The reconstruction algorithm is applied and compared to a direct fit to the simulated data for these materials in order to further validate the applicability of the developed procedure to a wide range of materials.

IV. RESULTS

A. Positron implantation profiles (PIPs)

The normalized PIP histograms for all 270 materials considered in this analysis can be found in the supplementary material. A representative set of these PIPs is plotted in Fig. 3 to better convey the spread in the entire dataset. Of particular note is the exponential character of the function over a wide range in depth, a feature previously obscured by the use of encapsulating foils for the source and that consequently required fitting of a piece-wise function to the PIP.[3] While there remains an atomic number dependency, the dominant differentiating point among these curves results from the material electronic density due to the fact that positrons lose energy quickly through ionization and core electron excitation. This is then followed by valence electron

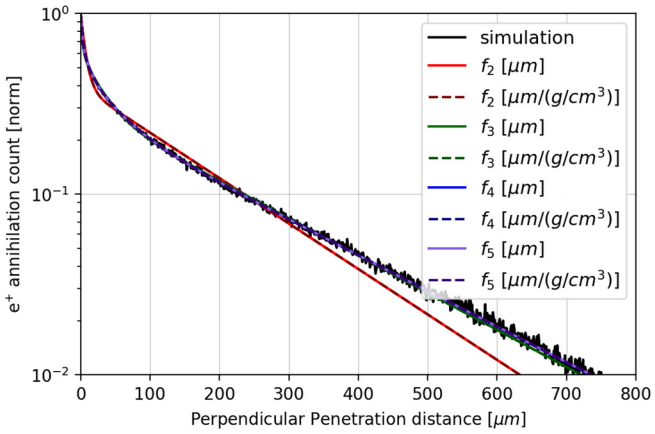

FIG. 5. Representative example of fit for all PIP functional forms considered with f_x indicating an x-term exponential fit, [μm] indicating a fit with respect to the distance, and [$\mu m/(g/cm^3)$] indicating a fit with respect to the distance divided by the density of the material of interest. It can be readily observed that the two-term and three-term exponential fits do not entirely capture all features in the PIP. These data are shown for a representative material (the ICRP definition of skeletal muscle) within the 270 material database published with the paper.

excitations and phonon emission as the positron approaches a thermal Maxwell–Boltzmann energy distribution.[2] Of additional utility is the PIP parallel to the material surface, as this determines the effective width of the sensitivity range. This is shown for a subset of materials in Fig. 4 for the common geometry in this set of simulations, as described in Sec. III. These histograms are also included in the supplementary material. As anticipated given the isotropic nature of the source, the parallel profile can extend non-trivially beyond the footprint of the ^{22}NaCl source cylinder in lower density materials. This should be considered for applications such as characterization of damage resulting from ion implantation doping if defect concentrations are to be derived from a PAS technique.

B. PIP fitting

Given the potentially limited utility of the PIP database for materials beyond its scope, a parameterization of a fitting function is conducted. Two-term, three-term, four-term, and five-term exponentials are considered, as discussed in Sec. III. Each new functional term contributes two additional parameters to the fit—the vertical-axis intercept coefficient and the characteristic slope of each exponential. A representative example of a simulated PIP (the ICRP definition of skeletal muscle) and the obtained fit results for all models considered are shown in Fig. 5.

The resulting goodness-of-fit metrics for all functional forms applied to all 270 materials in the database constructed in the effort are shown in Fig. 6. According to all fit quality metrics, the four-term fit is found to be superior to the two-term and three-term exponential fits, while the addition of the 5th term does not substantially improve the fit quality. The fit residuals are also analyzed in Fig. 7, with a fit being considered of high quality if there remains no apparent trends in the residuals. This would indicate that all of the PIP's features have been adequately captured in the fit. It is seen that trends remain in the residuals for the two-term and three-term exponential fits, particularly at short positron penetration distances, further confirming their inferior quality. The four-term fit as a function of distance [f_4 (μm)] is shown to be the minimally complex model, which adequately characterizes the PIP; as such, this model is selected as the model of choice.

The Shapiro–Wilk test, the common normality test with the highest power, is used to statistically test the residuals for

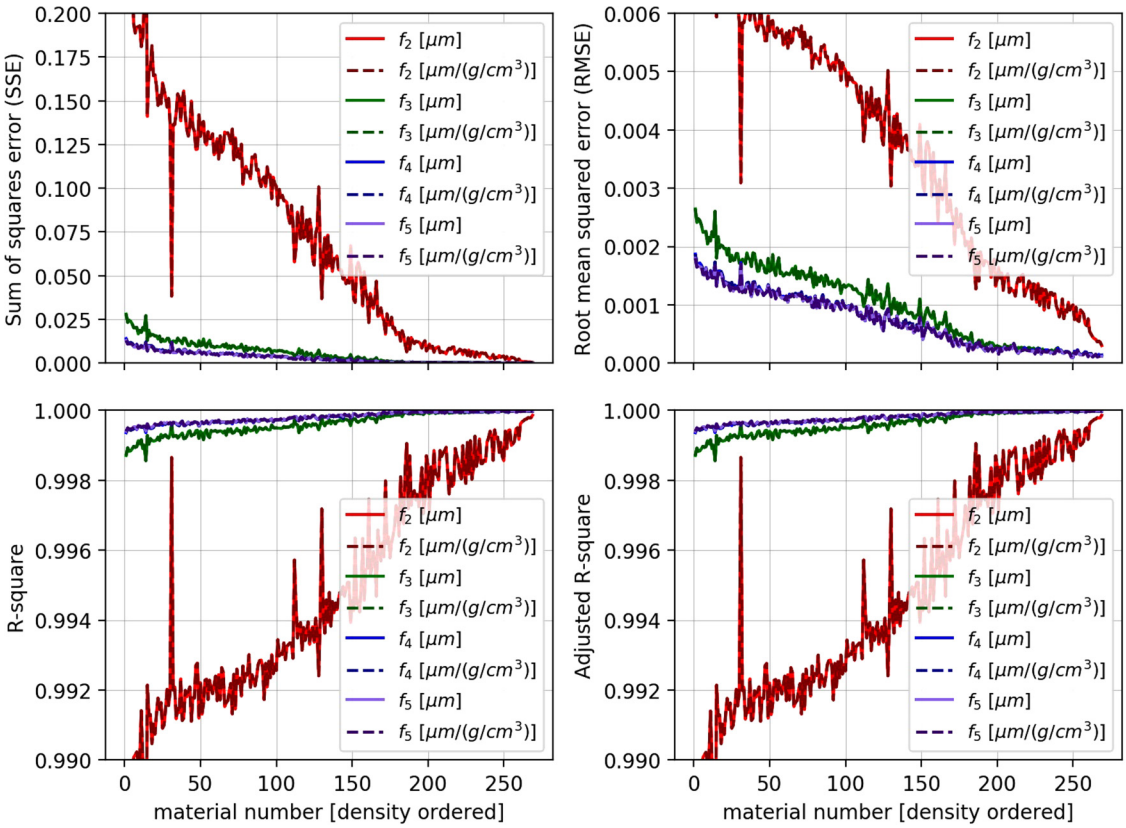

FIG. 6. Quantification of goodness-of-fit for all PIP functional forms considered, with f_x indicating an x-term exponential fit. [μm] indicates a fit with respect to the distance, and [μm/(g/cm^3)] indicates a fit with respect to the distance divided by the density of the material of interest. It is shown that two-term and three-term exponential fits provide inferior quality according to all goodness-of-fit parameters, while the addition of the fifth term does not substantially improve the fit quality.

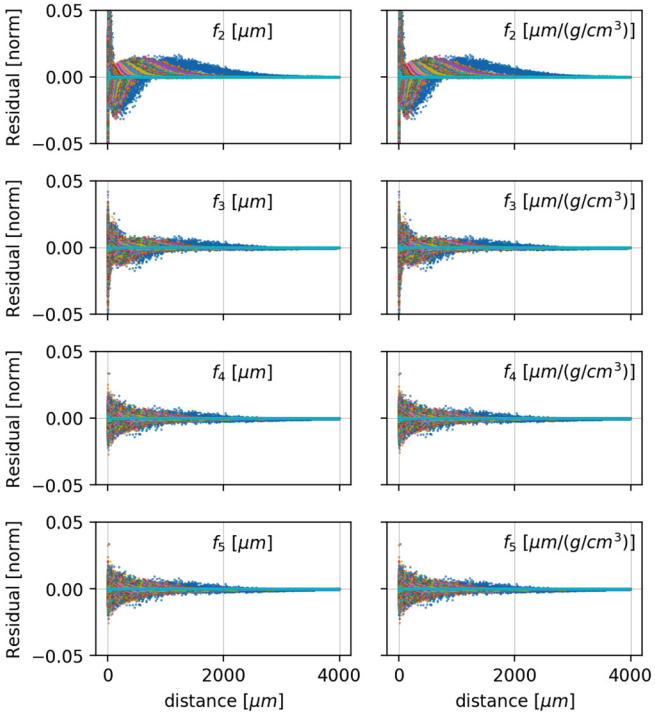

FIG. 7. Quantification of fit residuals for all PIP functional forms considered, with f_x indicating an x-term exponential fit. [μm] indicates a fit with respect to the distance, and [μm/(g/cm^3)] indicates a fit with respect to the distance divided by the density of the material of interest. Similar to Fig. 6, it can be seen that the two-term and three-term fits are inferior due to observable trends in their residuals, while the five-term fit does not noticeably improve upon the four-term fit.

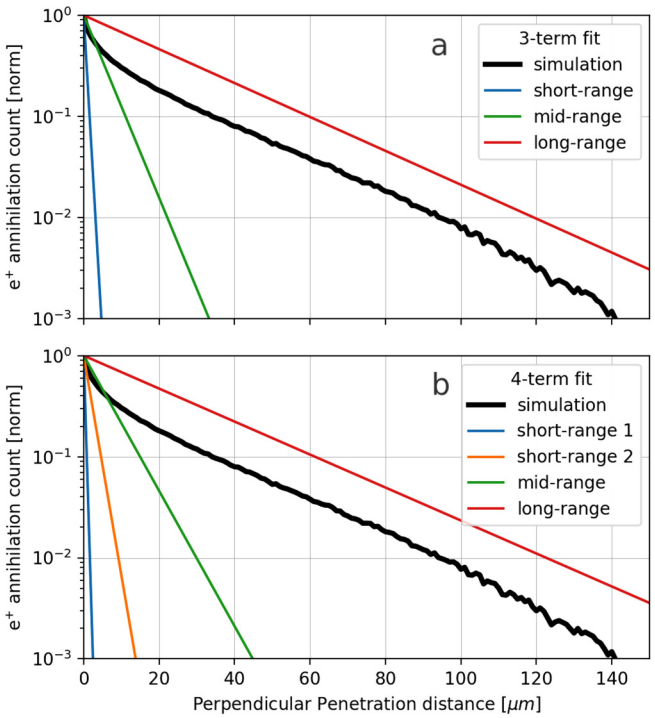

FIG. 8. Contribution of each of the characteristic slope terms in the exponential fit for three-term (a) and four-term (b) fits of the positron implantation profile in stainless steel. It is observed that both fits have one dominant long-range term (red) and one dominant mid-range term (green), but that the four-term fit has two short-range term contributions, while the three-term fit has only one. This difference explains why superior fits at a short range are found for the four-term fit and trends in the residuals are removed, as shown in Fig. 7.

normality.[34,35] It is found that over the fractional range from 95% to 50%, with a p-value of 0.05, one fails to reject the null hypothesis and concludes that no significant departure from normality is present in the residuals. This is untrue for the three-term fit, as shown in the supplementary material. While the three-term fit is sufficient to model the bulk curvature of the PIP, the four-term fit is required to precisely model the low-distance curvature, as is necessary if PAS is to accurately characterize damage produced by low-penetration heavy ions. The four-term fit as a function of distance [f_4 (μm)] is selected over f_4 [μm/(g/cm^3)] due to the equivalent quality of the fit and the ease for model users in employing a non-transformed, independent variable. The functional form of this model is given in Eq. (7). The parameters for this model obtained for all materials in the 270 material database can be found in the supplementary material.

From this representative example in Fig. 5, the goodness-of-fit metric, and the residual-based determination of fit quality, the sufficiency of the four-term fit as a function of distance [f_4 [μm]] can be visually confirmed.

To further justify the necessity of the fourth exponential term, the contribution of each of the characteristic slope terms is shown in Fig. 8 for a representative material (stainless steel). It is observed that within the four-term fit, two terms contribute to matching the PIP curvature at a short range, one contributes to a mid-range, and one contributes to a long range. The characteristic slope of the long-range term corresponds to the commonly cited attenuation coefficient. The three-term fit neglects one of the short-range terms, which causes the remaining trends in the residuals of these fits, as observed in Fig. 7. This is of particular import for ion implantation damage studies because high linear-energy-transfer ions deposit all of their energy in this shallow penetration region. Furthermore, for all PAS studies, these short distances are where the maximum part of the measured signal originates.

Figure 9 compares the model developed in this effort to previous models [Eqs. (1)–(6)]. Figure 9(a) represents the PIP for Kapton directly from GEANT4 simulation, from published models, and from the model proposed in this effort. Kapton is chosen because many of the historic models were developed for use with Kapton due to its frequent use as a source encapsulation material. The model presented in this effort is best able to capture the simulated PIP at all length scales. Gleason's formula has been found experimentally to err significantly for nonmetals.[10] The importance of the good agreement at small

length scales is illustrated in Fig. 9(b). SRIM calculations are conducted to predict the vacancy concentration as a function of depth for 18.5 MeV Xe^{26+} ions, an irradiation scenario for which conventional PALS has been used in the literature.[36] This vacancy profile is weighted with the PIP to form the effective vacancy concentration, which is measured in PAS. The annihilation weighted vacancy concentration is plotted in Fig. 9(b), for all models considered in Fig. 9(a). The percent error of the integral of these curves with respect to the simulation is given in the legend. The significant errors (exceeding 40% for the majority of fits considered) illustrate the importance of an accurate parameterization of the PIP at a short range.

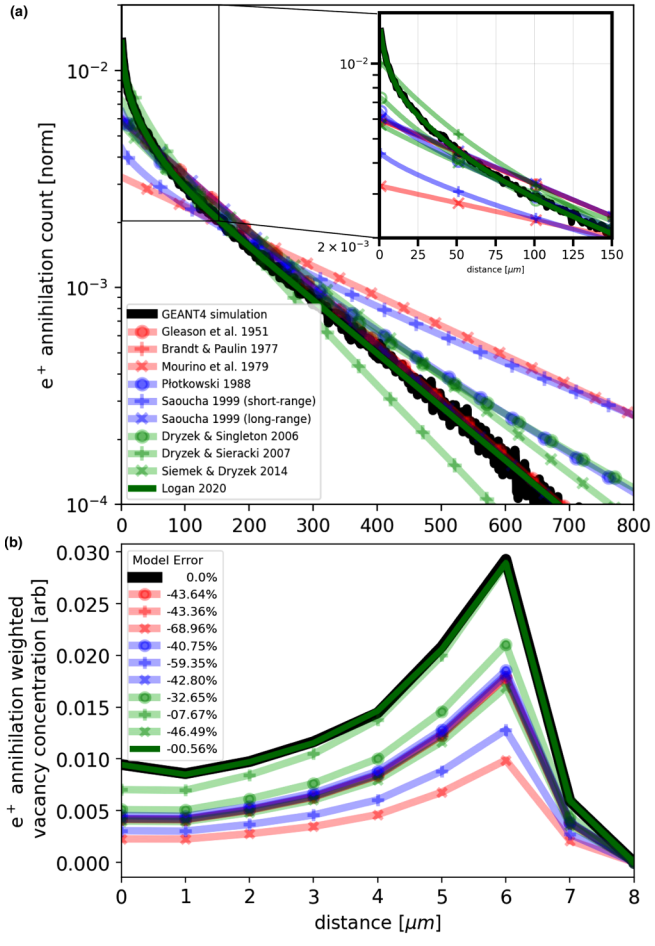

FIG. 9. (a) Comparison of various PIP models [Eqs. (1)–(6)] with GEANT4 simulation of the positron implantation profile (the inset figure at a short range) in Kapton. The model proposed in this effort is the most capable of matching the GEANT4 curve at all length scales. (b) PIP-weighted, heavy-ion-produced vacancy concentration in Kapton. The vacancies are representative of incident 18.5 MeV Xe^{26+} ions, which PAS has been used to study.[36] The PIP models are those used in (a). The legend gives the error of each model with respect to the GEANT4 results, in terms of integral underneath the positron-measured damage curve. The model that we propose leads to experiment interpretation with the least error.

C. Element-based, all-material PIP construction algorithm

A reconstruction algorithm is developed in order to derive the PIPs of materials outside the database published in this effort. The inputs of this reconstruction algorithm are the PIP parameters for the four-term exponential fit as a function of distance [f_4 (μm)] for all pure elements simulated at a density of 4 g/cm^3 to best approximate the densities of most materials of interest. Although density differences are corrected in the reconstruction algorithm, this density equalization was found to improve model results. The algorithm for reconstructing the exponential characteristic slope parameters C_i^a [B, D, F, and H in Eq. (7)] is given in Eq. (8),

$$C_i^a = \sum_k C_i^k f_k \frac{\rho^a}{\rho_k}, \tag{8}$$

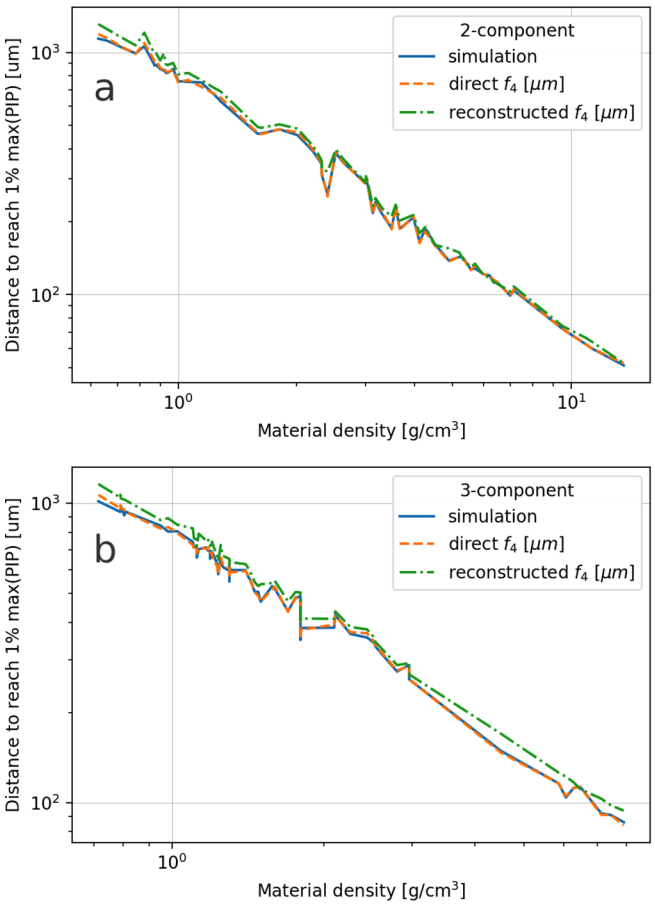

FIG. 10. Demonstration of direct simulation, direct four-term fit as a function of distance [f_4 [μm]] and a reconstructed four-term fit as a function of distance [f_4 [μm]] prediction of the penetration distance into the material at which 99% of positrons have already annihilated for all binary (a) and ternary (b) compounds within the 270 material database of PIPs published with this paper. There is observed to be excellent agreement between the predictions, indicating adequacy of the reconstruction algorithm published for binary and ternary compounds.

and the algorithm for reconstructing vertical-axis intercept coefficient parameters C_i^a [A, C, E, and G in Eq. (7)] is given in Eq. (9),

$$C_i^a = \sum_k C_i^k f_k, \tag{9}$$

where f_k is the mass percentage of the element k in the material of interest a, ρ^a is the density of the material of interest a, and $\overline{\rho_k}$ is the average density of the elements in the reconstruction (here $4\,\mathrm{g/cm^3}$ by default). The sum is conducted for all elemental constituents k of the material, which have coefficients C_i^k, as given in the supplementary material.

Practically, the one major experimental utility of this parameterization is to enable determination of the PAS technique sensitivity range in any arbitrary material. To quantify the accuracy of this reconstruction technique for this purpose, the distance at which 1% of positrons penetrate without annihilation is quantified directly from simulation, from a direct four-term exponential fit as a function of distance [f_4 (μm)] to these data, and from the reconstruction algorithm presented in Eqs. (8) and (9) for all binary and ternary compounds (Fig. 10) in the database published with this paper. The average fractional error in this quantity is 6.7% for binary compounds and 7.9% for ternary compounds, showing the sufficiency of this reconstruction algorithm for experimental utility.

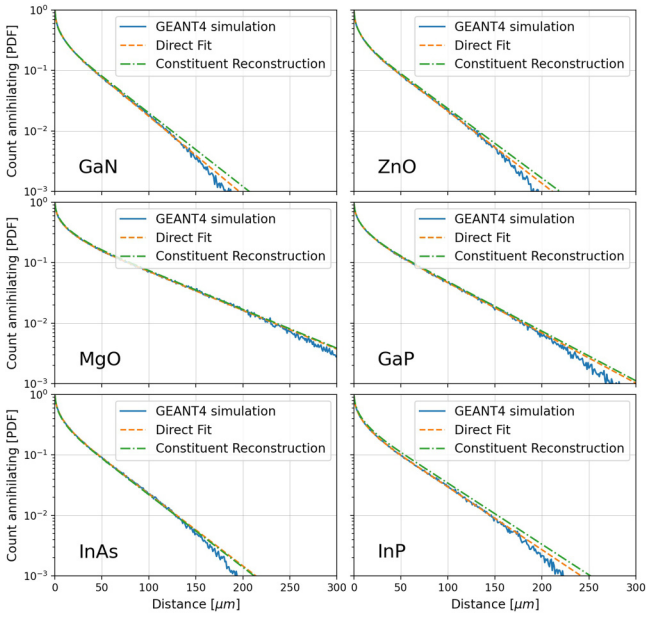

FIG. 11. Demonstration of direct simulation, direct four-term fit as a function of distance [f_4 (μm)] and a reconstructed four-term fit as a function of distance [f_4 (μm)] from elemental information of six semiconductors, which are often analyzed using PAS-based techniques. This demonstrates the utility of the reconstruction algorithm in reliably producing a PIP for an arbitrary material.

To demonstrate this utility, the results of the direct simulation, direct fit to the simulation, and reconstruction from only elemental information for six semiconductors often characterized through PAS-based techniques can be found in Fig. 11. The excellent agreement is clearly visible with the maximum percent error being 8% for InP, associated with an error of $4\,\mu$m.

V. CONCLUSION

A more accurate positron implantation profile (PIP) is constructed for the radioactive decay of ^{22}Na (the dominant radionuclide used in PAS techniques) for any arbitrary material of interest. As this quantity determines the sensitivity range for all non-slow PAS-based characterization methods, this profile is of wide practical utility. It is shown that rather than the commonly employed two-term (four parameter) exponential fit in the literature, an improved four-term (eight parameter) fit as a function of distance [f_4 (μm)] provides the best parameterization of all materials of interest. These eight parameters as well as the simulated PIP data are published with this paper for a set of 270 materials, serving as a useful reference for experimentalists. Furthermore, an algorithm is presented to transform elemental PIPs into those for any arbitrary material, thus allowing for the derivation of the PIP for any arbitrary material of interest even if it is not within the database hereto mentioned. This parameterization will serve to improve the experimental design and analysis accuracy for PAS techniques independent of the material being characterized.

SUPPLEMENTARY MATERIAL

See the supplementary material for (1) elemental parameterization data for reconstruction of arbitrary material PIPs, (2) parameterization data for the 270 material database considered in this analysis, and (3) raw histograms ($1\,\mu$m bin width) of positron annihilation positions in X/Y (parallel to the sample surface) and Z (perpendicular to the sample surface) for 1 000 000 simulated positrons in GEANT4. Also included are analyses of the fit results obtained with different fitting algorithms (reversing the order and applying different weights) as well as a more thorough comparison of the three-term and four-term fits.

ACKNOWLEDGMENTS

The present work has benefited from the financial support of the U.S. Department of Defense SMART Fellowship, as well as the financial support from the Air Force Research Laboratory Space Vehicles Directorate. Approved for public release. Public Affairs release approval AFMC-2020-0316.

APPENDIX: PHYSICS LIST VALIDATION

Figure 12 demonstrates that the use of the GEANT4 PENELOPE (PENetration and Energy LOss of Positrons and Electrons) and Shielding physics lists produces equivalent PIP results to within statistical variability.

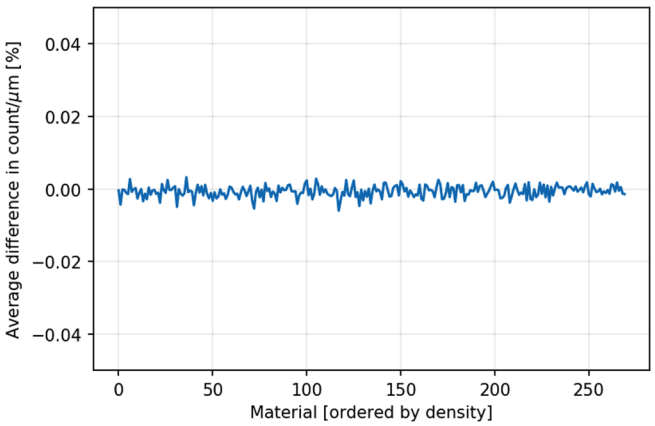

FIG. 12. Percent difference between material PIPs calculated using the GEANT4 PENELOPE (PENetration and Energy LOss of Positrons and Electrons) and Shielding physics lists. The results are seen to agree to within the statistical variation of this Monte Carlo particle transport code. While the PENELOPE physics list is employed in this effort, this validates the use of the Shielding physics list for purposes of PIP simulation.

DATA AVAILABILITY

The data that support the findings of this study are openly available in Zenodo at https://doi.org/10.5281/ZENODO.3741748, alongside the GEANT4 input files and MATLAB scripts used to carry out the calculations, Ref. 37.

REFERENCES

[1]M. Saro, V. Kršjak, M. Petriska, and V. Slugeň, AIP Conf. Proc. **2131**, 020039 (2019).
[2]K. Saarinen, in *III-Nitride Semiconductors: Electrical, Structural and Defects Properties*, edited by O. Manasreh (Elsevier, Amsterdam, 2000), pp. 109–149.
[3]J. Dryzek and D. Singleton, Nucl. Instrum. Methods Phys. Res. Sect. B **252**, 197 (2006).
[4]P. Horodek and J. Dryzek, Nukleonika **55**, 17 (2010).
[5]L. Dubov, Y. Akmalova, S. Stepanov, and Y. Shtotsky, Acta Phys. Pol. A **132**, 1482 (2017).
[6]J. Dryzek and P. Horodek, Nucl. Instrum. Methods Phys. Res. Sect. B **267**, 3580 (2009).
[7]S.-J. Huang, Z.-W. Pan, J.-D. Liu, R.-D. Han, and B.-J. Ye, Chin. Phys. B **24**, 107803 (2015).
[8]J. Dryzek, P. Horodek, and M. Dryzek, Appl. Phys. A **124**, 451 (2018).
[9]M. Mourino, H. Löbl, and R. Paulin, Phys. Lett. A **71**, 106 (1979).
[10]J. Dryzek, Acta Phys. Pol. A **107**, 598 (2005).
[11]V. Kršjak, J. Degmová, R. Lauko, J. Snopek, M. Saro, K. Sedlačková, S. Sojak, M. Petriska, G. Farkas, Y. Dai, and V. Slugen, Nucl. Instrum. Methods Phys. Res. Sect. B **434**, 73 (2018).
[12]M. J. Puska and R. M. Nieminen, Rev. Mod. Phys. **66**, 841 (1994).
[13]J. Dryzek, Acta Phys. Pol. A **137**, 196 (2020).
[14]G. F. Knoll, "Radiation interactions," in *Radiation Detection and Measurement* (John Wiley & Sons, Inc., 2000), Chap. 2, pp. 43–47.
[15]G. I. Gleason, J. D. Taylor, and D. L. Tabern, Nucleonics **8**, 12 (1951).
[16]W. Brandt and R. Paulin, Phys. Rev. B **15**, 2511 (1977).
[17]K. Płotkowski, T. Panek, and J. Kansy, Il Nuovo Cimento D **10**, 933–940 (1988).
[18]A. Saoucha, J. Appl. Phys. **85**, 1802 (1999).
[19]J. Dryzek and J. Sieracki, Nucl. Instrum. Methods Phys. Res. Sect. B **258**, 493 (2007).
[20]K. Siemek and J. Dryzek, Acta Phys. Pol. A **125**, 833 (2014).
[21]J. Kuriplach and B. Barbiellini, Phys. Rev. B **89**, 155111 (2014).
[22]S. Agostinelli, J. Allison, K. Amako, J. Apostolakis, H. Araujo, P. Arce, M. Asai, D. Axen, S. Banerjee, G. Barrand, F. Behner, L. Bellagamba, J. Boudreau, L. Broglia, A. Brunengo, H. Burkhardt, S. Chauvie, J. Chuma, R. Chytracek, G. Cooperman, G. Cosmo, P. Degtyarenko, A. Dell'Acqua, G. Depaola, D. Dietrich, R. Enami, A. Feliciello, C. Ferguson, H. Fesefeldt, G. Folger, F. Foppiano, A. Forti, S. Garelli, S. Giani, R. Giannitrapani, D. Gibin, J. J. Gomez Cadenas, I. Gonzalez, G. Gracia Abril, G. Greeniaus, W. Greiner, V. Grichine, A. Grossheim, S. Guatelli, P. Gumplinger, R. Hamatsu, K. Hashimoto, H. Hasui, A. Heikkinen, A. Howard, V. Ivanchenko, A. Johnson, F. W. Jones, J. Kallenbach, N. Kanaya, M. Kawabata, Y. Kawabata, M. Kawaguti, S. Kelner, P. Kent, A. Kimura, T. Kodama, R. Kokoulin, M. Kossov, H. Kurashige, E. Lamanna, T. Lampen, V. Lara, V. Lefebure, F. Lei, M. Liendl, W. Lockman, F. Longo, S. Magni, M. Maire, E. Medernach, K. Minamimoto, P. Mora de Freitas, Y. Morita, K. Murakami, M. Nagamatu, R. Nartallo, P. Nieminen, T. Nishimura, K. Ohtsubo, M. Okamura, S. O'Neale, Y. Oohata, K. Paech, J. Perl, A. Pfeiffer, M. G. Pia, F. Ranjard, A. Rybin, S. Sadilov, E. di Salvo, G. Santin, T. Sasaki, N. Savvas, Y. Sawada, S. Scherer, S. Sei, V. Sirotenko, D. Smith, N. Starkov, H. Stoecker, J. Sulkimo, M. Takahata, S. Tanaka, E. Tcherniaev, E. Safai Tehrani, M. Tropeano, P. Truscott, H. Uno, L. Urban, P. Urban, M. Verderi, A. Walkden, W. Wander, H. Weber, J. P. Wellisch, T. Wenaus, D. C. Williams, D. Wright, T. Yamada, H. Yoshida, and D. Zschiesche, Nucl. Instrum. Methods Phys. Res. Sect. A **506**, 250–303 (2003).
[23]M. Pia, Nucl. Phys. B Proc. Suppl. **125**, 60 (2003).
[24]G. A. P. Cirrone, G. Cuttone, S. Donadio, V. Grichine, S. Guatclli, P. Gumplinger, V. Ivanchenko, M. Maire, A. Mantero, B. Mascialino, P. Nieminen, L. Pandola, S. Parlati, A. Pfeiffer, M. G. Pia, and L. Urban, in *2003 IEEE Nuclear Science Symposium. Conference Record (IEEE Cat. No.03CH37515)* (IEEE, 2003), Vol. 1, pp. 482–485.
[25]J. Baró, J. Sempau, J. Fernández-Varea, and F. Salvat, Nucl. Instrum. Methods Phys. Res. Sect. B **100**, 31 (1995).
[26]S. Tanuma, C. J. Powell, and D. R. Penn, J. Appl. Phys. **103**, 063707 (2008).
[27]J. Dryzek and P. Horodek, Nucl. Instrum. Methods Phys. Res. Sect. B **266**, 4000 (2008).
[28]X. Lai, X. Jiang, X. Cao, X. Zhang, Z. Zhang, X. Cao, G. Xiang, B. Wang, and L. Wei, Surf. Interface Anal. **49**, 457 (2017).
[29]X. Ning, X. Cao, C. Li, D. Li, P. Zhang, Y. Gong, R. Xia, B. Wang, and L. Wei, Nucl. Instrum. Methods Phys. Res. Sect. B **397**, 75 (2017).
[30]X. Lai, X. Jiang, X. Cao, X. Zhang, Z. Zhang, X. Cao, G. Xiang, B. Wang, and L. Wei, Surf. Interface Anal. **49**, 457 (2016).
[31]C. Hugenschmidt, Surf. Sci. Rep. **71**, 547 (2016).
[32]K. Eckerman and A. Endo, Ann. ICRP **38**, 7 (2008).
[33]M. A. Branch, T. F. Coleman, and Y. Li, SIAM J. Sci. Comput. **21**, 1 (1999).
[34]S. S. Shapiro and M. B. Wilk, Biometrika **52**, 591 (1965).
[35]N. Mohd Razali and B. Yap, J. Stat. Model. Anal. **2**, 25 (2011).
[36]J. Dryzek, P. Horodek, and M. Dryzek, Appl. Phys. A **124**, 451 (2018).
[37]J. Logan and M. Short (2020). "2020-Universal-PIP," Zenodo. https://doi.org/10.5281/ZENODO.3741748.